Regions of the human renal artery: histomorphometric analysis

Blanca Mompeó-Corredera[1], Pablo Hernández-Morera[2], Irene Castaño-González[3],
María del Pino Quintana-Montesdeoca[4], Natalia Mederos-Real[5]

[1]Department of Morphology, University of Las Palmas de Gran Canaria, Las Palmas de Gran Canaria, [2]IUMA Information and Communication Systems, University of Las Palmas de Gran Canaria, Las Palmas de Gran Canaria, [3]Department of Dermatology, Doctor Negrin University Hospital of Gran Canaria, Las Palmas de Gran Canaria, [4]Department of Math, University of Las Palmas de Gran Canaria, Las Palmas de Gran Canaria, [5]Department of Forensic Pathology, Institute of Legal Medicine of Las Palmas, Las Palmas de Gran Canaria, Spain

Abstract: The renal artery is frequently involved in the pathogenesis of vasculorenal diseases, and it is a target in kidney surgery and therapeutic techniques for refractory hypertension. However, few detailed structural studies on the human renal artery have been conducted. Using histocytochemistry, immunohistochemistry, and quantitative image analysis, the wall thickness, structure, smooth muscle cells, extracellular matrix, and proportion of elastic tissue in the tunica media of main human renal arteries were used estimated. Ninety-six tissue samples were collected from sections of the right and left main renal arteries. The results showed that the renal artery changed from an elastic vessel in its proximal segment to a muscular artery in its distal part. A critical characteristic of the renal artery was the presence of longitudinal smooth muscle cell formations in the tunica adventitia of middle and distal segments but not in the proximal part of the artery. In addition, the tunica adventitia of the renal artery showed a rich vascularization and the presence of numerous nerves profiles. The artery's regional structural and morphometric features explain that a particular arterial pathology is more frequent in a specific vessel sector than in others. In addition, those characteristics could determine a different therapeutic response attending to the arterial sector.

Key words: Renal artery, Morphometry, Immunohistochemistry, Smooth muscle, Extracellular matrix

Introduction

Kidney transplantation surgery, in which vascular abnormalities account for dysfunction in up to 10% of the renal transplanted patients at any time after graft placement [1], and the use of current techniques for treating refractory hypertension make the renal artery growing in relevance.

Angioplasty to repair renal artery stenosis [2-4] renal denervation to control sympathetic arterial activity, including catheter-based renal denervation [5-7] and renal artery adventitia stripping [8] are all techniques currently considered for the control of refractory hypertension. These techniques act on the main renal artery as the target.

However, along with recent studies in which renal artery characterization was not the main object of the research, and only a specific part of the artery was scrutinized, studies focusing on the renal artery's structural characteristics are scarce. These studies include little more than the analysis of the human renal artery in the context of a histological examination of the peripheral arteries [9], the description of its ultrastructure in the rat during growth and aging [10], and some studies carried out on the transitional zone of the renal artery [11, 12].

Corresponding author:
Blanca Mompeó-Corredera 🔾
Department of Morphology, University of Las Palmas de Gran Canaria,
Las Palmas de Gran Canaria 35016, Spain
E-mail: blanca.mompeo@ulpgc.es

The main renal artery is a conduit artery that appears at approximately 6 to 7 weeks of prenatal development in humans [13, 14] and supplies around 20% of the cardiac output to the kidney. The length and diameter of this artery vary with the side age and sex [15]. Variations in the number of renal arteries that arrive at a kidney are frequent and occur in approximately 30% of kidneys [16-18]. The multiple renal arteries originate in the lateral aspect of the aorta, iliac arteries even in the testicular arteries [19].

The mammalian arteries are usually classified as elastic or muscular arteries, depending on the histological characteristics of the tunica media; both types of vessels differ in structure, production of nitric oxide, and Ca++ channels [20]. Therefore, the physiological and pathological arterial characteristics depend on the amount of elastic, fibrous, and muscular components in the tunica media.

According to the type, elastic arteries are more prone to atherosclerosis than are muscular arteries. Moreover, arterial stiffening due to aging is more prominent in elastic arteries [20, 21]; meanwhile, the muscle arteries' stiffness leads to an increase in vascular tone, which can be influenced by vasoactive mediators [22].

Wright in human renal arteries [9] and Osborne-Pellegrin [10] in rat renal arteries described variations in its structure from the proximal to the distal segment. Therefore, renal artery pathological stenosis would be produced by different pathologic processes depending on the affected arterial segment so that the therapeutic approach may be different.

This work aims to characterize the renal arterial wall along its length, assess the fraction of extracellular matrix, elastic component, and smooth muscle cells (SMCs) in the tunica media of different sections of the artery, and compare the fraction of those components in the distinct segments, as well as to discuss the possible consequences of any variations on vascular pathology and therapeutic procedures to the artery.

Materials and Methods

Study material

Thirty-two main renal arteries from the aorta to renal hilus were obtained from 16 cadavers (14 male and two female) aged 14–75 years (Table 1). Cadaverswerenecropsied in the Instituto de Medicina Legal de Las Palmas de Gran Canaria. The arteries were removed in a block from the corpses, dissected and sectioned.

Tissue preparation

The right and left renal arteries were circumferentially cross-sectioned in three-thirds (proximal, middle, and distal) (Table 1) and fixed by immersion in neutral buffered 10% formalin. A total of 96 tissue samples were processed for histological and immunohistological studies. After fixation, the samples were dehydrated through graded alcohols and embedded in paraffin wax. One tissue block was made from each arterial segment, and consecutive transverse sections of 5μm thickness were obtained from each paraffin block.

Sections were stained with the following techniques: hematoxylin-eosin, Masson's trichrome, and resorcin using routine methods in our lab.

For immunohistochemistry studies, sections were immunolabeled with anti-von Willebrand factor, anti-actin, and anti-S100 neuronal antibodies. The immunohistochemical methodology is summarized in Table 2.

Von Willebrand factor immunodetection was performed with an anti-human polyclonal anti-factor VIII-related antibody produced in rabbits at a dilution of 1:100. In addition, an anti-human monoclonal anti-actin alpha-smooth muscle antibody produced in mice, diluted 1:2,000, was utilized for actin immunodetection. For S100 detection, an anti-human monoclonal S100 antibody was produced in rabbits; a 1:300 dilution was used. In all cases, endogenous peroxidase was blocked with 3% hydrogen peroxide for 30 minutes in methanol.

Samples were analyzed with a Labophot-2 Nikon micro-

Table 1. Characteristics of the study sample

Characteristic	Value
Age groups[a]	
14–29 yr	3 male
30–50 yr	5 male
51–75 yr	6 male+2 female
Arterial segment[b]	
Proximal	32 (34.0)
Right	16 (34.0)
Left	16 (34.0)
Middle	31 (33.0)
Right	16 (34.0)
Left	15 (31.9)
Distal	31 (33.0)
Right	15 (31.9)
Left	16 (34.0)
Total	94 (100)
Right	47 (100)
Left	47 (100)

Values are presented as number (%). [a]Sex distribution according to age groups. [b]Distribution of renal arteries side according to the arterial segment.

Table 2. Summary of immunohistochemical methodology

Antibody	Source	RRID	Host	Type	Clone	Antigen retrieval	Dilution
Anti-S100	Thermo Fisher, Waltham, MA, USA	AB_10979153	Rabbit	Polyclonal	-	0.1% trypsin[b]	1:300
Anti- Actin	Sigma-Aldrich, St. Louis, MO, USA	AB_262054	Mouse	Monoclonal	Anti-actin alpha-smooth muscle-antibody-1A4	0.1% trypsin[a]	1:2,000[c]
Factor VIII	Zymed	AB_2811207	Rabbit	Polyclonal		Trypsin[a]	1:100[c]

RRID, research resource identifiers. [a]0.1%Tripsina, 60 min at 37°C, [b]0.1%Tripsina, 10 min at 37°C, [c]1% goat serum in saline phosphate buffer, 4°C overnight.

scope (Badhoevedorop, The Netherlands), and a Sight DS-5 M digital camera (Nikon Digital Sight DS-5M-L1; Melville, NY, USA) captured images at 2×, 4×, 10×, and 100× magnification. The descriptive, structural analysis was always done in the healthy part of each sector of the arterial wall, avoiding destructured zones, calcifications, and pathologic thicknesses if they were present.

Measurements of the arterial wall thickness

The arterial wall thickness tunica intima and media (IM), tunica media, and tunica intima were measured in transverse histological sections. Measurements were performed in selected fields of one Masson trichrome-stained histological section of each case using a Digital Sight Camera Control Unit (Nikon Digital Sight DS-5M-L1) coupled to a Labophot-2 Nikon microscope. Four different measurements were performed directly in each histological section using digital camera tools. The arterial sections were divided into four-quadrant. Measurements were done in each of the four quadrants, always avoiding damaged tissue if it was present. The median of the four sizes was considered the value of the measure. The tunica media thickness was considered to be the perpendicular stretch between the innermost and outermost elastic lamina. The tunica adventitia was not measured because it was not possible to determine the outer limit of this tunica in all cases.

Quantification of the components of the arterial wall

The quantification of the structural elements of the arterial wall was measured in the arterial tunica media. The elastic tissue was assessed between the inner and outer elastic membrane without the inclusion of those.

Photographs (4×) from the samples stained with Masson's trichrome were used to quantify the SMCs and extracellular matrix composition in the tunica media. Photographs (10×) of the samples stained with resorcin stain were used for the determination of the elastic component in the tunica media between the inner and the outer elastic lamina, avoiding those laminas.

Quantification of the fraction of elastin

Each delimited image was converted to grayscale and then binarized by a high threshold value resulting in a binary image, in which the media layer appears as a white object over a black background [22]. The resulting image defines the portion of the original image corresponding to the media layer of the vessel wall.

In a binary image, the white color is coded with the value 1, and the black color is coded with 0. Therefore, the media layer area identified by the white color can be calculated in pixels as the sum of all the pixels of the image.

On the other hand, each delimited image was binarized with a global threshold that could be adjusted interactively, allowing user to determine the threshold that properly segmented the elastin fibers (FE). The quantitative information extracted was the sum of pixels of the segmented objects in the resulting image of the elastin fiber segmentation. To compare measurements between different samples, the above amount was normalized by the sum of pixels of the media layer area computed previously, according to the following formula:

$$\%FE = \frac{Elastin\ fibers\ area}{Media\ layer\ area} \qquad (1)$$

The segmentation method was implemented using the numerical computing software MATLAB/Simulink Version R2019a (MathWorks, Natick, MA, USA).

Quantification of the muscular and extracellular matrix

First, the color image is converted to grayscale and then binarized by a high threshold value, resulting in a binary image, in which the inner and outer contours of the media layer were delimited to define the study area [22]. The media layer appeared as a white object over a black background, and the

media layer area was calculated in pixels as the sum of all the pixels of the binarized image.

Second, the color vessel wall image was clustered automatically in a predefined number of color-based classes. The smooth muscular fibers (SMF), and extracellular matrix components (ECM) of the vessel wall were grouped by a clustering algorithm based on the similarity between colors. The clustering algorithm used was a variation of the k-means [23-26], in which the similarity measure between two pixels, px_1 and px_2, is based on the distance calculated by the following expression:

$$distance\left(px_1, px_2\right) = \sqrt{w_1 \cdot \left(R_2 - R_1\right)^2 + w_2 \cdot \left(G_2 - G_1\right)^2 + w_3 \cdot \left(B_2 - B_1\right)^2} \quad (2)$$

where R_1, G_1, and B_1 are the color components of pixel px_1, and w_1, w_2, and w_3 are the weights that regulate the importance of each color component.

The number of groups k for the clustering algorithm was set at three with the aim of grouping the pixels corresponding to SMF, to ECM, and to the background image. The weights were determined heuristically as $w_1=2$, $w_2=1$, and $w_3=2$. The results were several black and white images, one per cluster, with the segmented vessel wall component, allowing us to calculate its extension. The third group of pixels corresponding to the background image was discarded.

The area in pixels of any component was computed by the sum of pixels of the segmented objects in the black and white images of each component. In this way, we obtained two measurements: A_{SMF}, the area in pixels of the SMF component, and A_{ECM}, the area in pixels of the ECM component.

The percentage of the total area of the media layer that was taken up by a component was calculated using the following formulas:

$$\%SMF = \frac{A_{SMF}}{Media\ layer\ area} \quad \%ECM = \frac{A_{ECM}}{Media\ layer\ area} \quad (3)$$

Statistical analysis

Data were analyzed using IBM SPSS Statistics ver. 27.0 (released 2020, for Windows; IBM Corp., Armonk, NY, USA). Categorical variables are expressed as frequencies and percentages. To analyze the association of two categorical variables, the chi-squared test was used. Numerical variables are summarized using the median and interquartile range (IR). Normality was considered according to the results of the Kolmogorov–Smirnov or Shapiro–Wilk tests. The 95% confidence interval (CI) is given in any case. To compare numerical variables of two independent samples, the nonparametric Mann–Whitney U test was used. For more than two independent samples, one-way ANOVA or the nonparametric Kruskal–Wallis test was used. Results are considered statistically significant if $P<0.05$.

Ethical approval

The Ethical Committee of the University of Las Palmas de Gran Canaria approved this research project (reference CEIH-2022-01), and the Formation and Research Committee of the Instituto de Medicina Legal y CienciasForenses de Las Palmas (IMLCF-Gobierno de Canarias) accredited that obtaining human samples followed the ethics and legal requirements.

Results

Histological and morphometric evaluation of the renal artery wall

The IM thickness was 493.6 μm (IR=285 μm) (Table 3). The boundary between the tunica intima and tunica media was well defined along the artery for an inner elastic membrane. The tunica media and tunica adventitia boundary was consistently well represented in all vessel sectors due to the morphological differences between the two tunica. The tunica media was formed by concentric layers of SMCs, different amounts of extracellular matrix, and elastic laminas, which had diverse dispositions depending on the arterial sector. The outer elastic membrane was considered to have two or more concentric elastic layers located between the tunica media and the tunica adventitia.

Although the left IM thickness was slightly wider than the right IM thickness, there was no significant difference between them. However, a significant difference was observed between the proximal and the other two arterial segments (Table 3).

Tunica intima

The tunica intima was constituted by endothelium and underlying connective tissue. In some cases, SMCs longitudinally disposed of could be observed. The thickness of the measured tunica intima was 40.2 μm (IR=143.5 μm), reaching the highest values in damaged zones and because of the

Table 3. Results of the wall thickness depending on the side and the arterial segment

Arterial segment	Wall thickness (µm)	P-value	Intima thickness (µm)	P-value	Media thickness (µm)	P-value
Median (IR)	493.6 (285)		40.2 (143.5)		441.8 (190.1)	
95% CI (mean)	517.4–634.1		61–119.8		448–525.9	
Number of arterial sections	94		94		94	
Right		0.382		0.358		0.533
Median (IR)	488.2 (265.8)		40.3 (59.0)		423.6 (255.1)	
95% CI (mean)	[471.4–610.6]		47.2–87		413.6–534.9	
Number of arterial sections	47		47		47	
Left						
Median (IR)	506.1 (246.6)		39.6 (114.7)		450.6 (173.2)	
95% CI (mean)	515.1–705.9		58–169.4		448.7–550.5	
Number of arterial sections	47		47		47	
Proximal		0.001*		<0.001*		0.053
Median (IR)	600.6 (406.2)		110.5 (152.9)		502.4 (376)	
95% CI (mean)	591.3–867.6		99.1–254.7		467.8–638	
Number of arterial sections	32		32		32	
Middle						
Median (IR)	451.6 (180.5)	0.679[a]	30.9 (22.2)	0.759[a]	418.8 (128.2)	
95% CI (mean)	426.6–545.1	0.001[b],*	28.5–60	<0.001[b],*	393.8–497.1	
Number of arterial sections	31		31		31	
Distal						
Median (IR)	470 (211.3)		33.3 (36.8)		437.3 (162)	
95% CI (mean)	438–576	0.003[c],*	31.6–62.7	<0.001[c],*	399.5–521	
Number of arterial sections	31		31		31	

Values are presented as the median (IR) and the 95% CI for mean. IR, interquartile range; CI, confidence interval. [a]P-value (Middle-Distal); [b]P-value (Middle-Proximal); [c]P-value (Distal-Proximal). *Statistically significant ($P<0.05$).
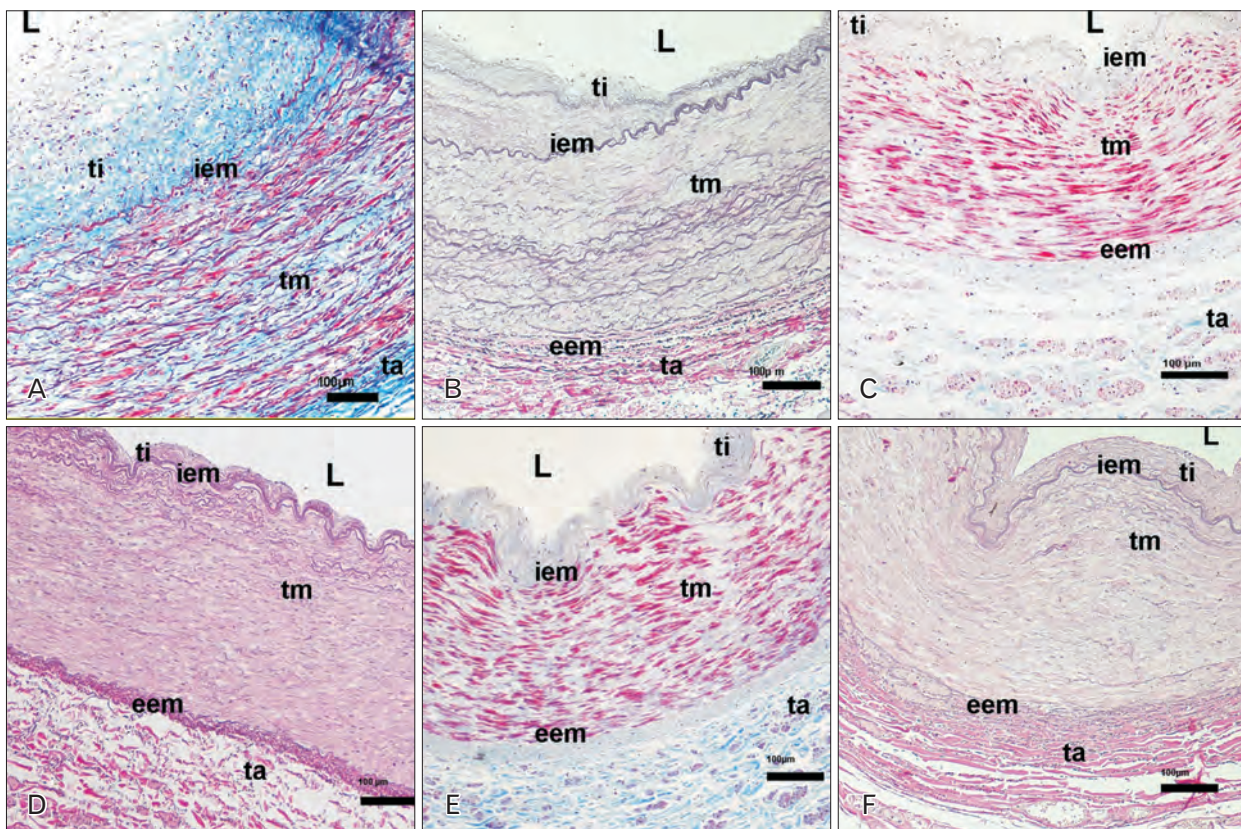

Fig. 1. Photomicrograph of the human renal artery wall. (A) Masson's trichromic stain, proximal segment; (B) resorcin stain, proximal segment; (C) Masson's trichromic stain, middle segment; (D) resorcin stain, middle; (E) Masson's trichromic stain, distal segment; and (F) resorcin stain, distal segment (bar=100 µm). L, lumen; ti, tunica intima; tm, tunica media; ta, tunicaadventitia; iem, internalelastic lamina; eem, externalelastic lamina.

Table 4. Percentage of the components in the tunica media attending to the side and the arterial segment

Arterial segment	Extracellular space (%ECM)	P-value	Elastin (%FE)	P-value	Smooth muscle cells (%SMF)	P-value
Median (IR)	73.4 (14.2)		12.2 (12.1)		25.1 (13.2)	
95% CI (mean)	68.9–73.7		13–17.1		25.3–29.7	
Number of arterial sections	87		83		87	
Right		0.209		0.092		0.647
Median (IR)	71.7 (16.4)		10.7 (11.2)		24.3 (12.5)	
95% CI (mean)	66.1–73.4		10.8–16.7		25.2–31.5	
Number of arterial sections	43		42		43	
Left						
Median (IR)	74 (13.6)		15.7 (11.6)		25.4 (13.4)	
95% CI (mean)	70–76.1		13.5–19.3		23.5–29.7	
Number of arterial sections	44		41		44	
Proximal		0.049*		<0.001*		0.056
Median (IR)	71.2 (16.4)		21.5 (14.7)		26 (12.6)	
95% CI (mean)	65.3–73.6	0.034[a],*	18.2–25.7	<0.001[a],*	24.8–31.3	
Number of arterial sections	31		30		31	
Middle		0.943[b]		<0.001[b],*		
Median (IR)	77 (12.2)		10.8 (12)		23 (11.8)	
95% CI (mean)	72.3–78.9		9.7–15.3		20.7–27	
Number of arterial sections	30	0.036[c],*	28	0.429[c]	30	
Distal						
Median (IR)	71.9 (16.3)		8.8 (5.4)		28.2 (15.5)	
95% CI (mean)	64.1–73.8		7.9–11.5		26–36	
Number of arterial sections	27		25		27	

Values are presented as the median (IR) and the 95% CI for mean. ECM, extracellular matrix components; FE, elastin fibers; SMF, smooth muscular fibers; IR, interquartile range; CI, confidence interval. [a]P-value (Proximal-Middle); [b]P-value (Proximal-Distal); [c]P-value (Middle-Distal). *Statistically significant (P<0.05).

presence of any pad. The tunica intima in our samples was significantly more expansive in the proximal arterial segment than in the other more distal arterial parts (Fig. 1, Table 3).

Tunica media

The thickness of the tunica media was 441.8 μm (IR=190.1 μm). There was no difference between the tunica media on the right and left renal arteries.

In the proximal third of the artery, the tunica media contained elastic layers running parallel to the SMC layers. Nevertheless, one external elastic membrane was not well defined (Fig. 1A, B).

The middle third of the artery showed well-defined inner and outer elastic membranes.

The tunica media was composed of SMCs and an extracellular matrix. In addition, some elastic laminas and smaller elastin plates were scattered in the spaces between muscle cells (Fig. 1C, D).

The tunica media of the distal third of the renal artery showed the presence of well-defined internal and external elastic membranes, limiting the tunica media from the tunica intima and tunica adventitia, respectively. Thus, the tu-

Table 5. Presence and missing of bunches of longitudinal smooth muscle cells in the tunica adventitia

	With SMC	Without SMC	Total	P-value
Total	36 (38.3)	58 (61.7)	94 (100)	
Right (n=47)	21 (44.7)	26 (55.3)	47 (100)	0.144
Left (n=47)	15 (31.9)	32 (68.1)	47 (100)	
Proximal (n=32)	1 (3.1)	31 (96.9)	32 (100)	<0.001*
Middle (n=31)	15 (48.4)	16 (51.6)	31 (100)	
Distal (n=31)	20 (64.5)	11 (35.5)	31 (100)	

Values are presented as number (%). SMC, smooth muscle cells. *Statistically significant (P<0.05).

nica media mainly comprises SMCs and connective matrix, with elastic laminas scarcely observed, and only small plates of elastic tissue present (Fig. 1E, F).

Components of the tunica media

The proportion of SMCs in the tunica media was 25.1% (IR=13.2%). There was no significant difference between the right and left renal arteries or the studied segments. However, a slight, no significant decrease in the muscular component was observed in the middle segment (Table 4).

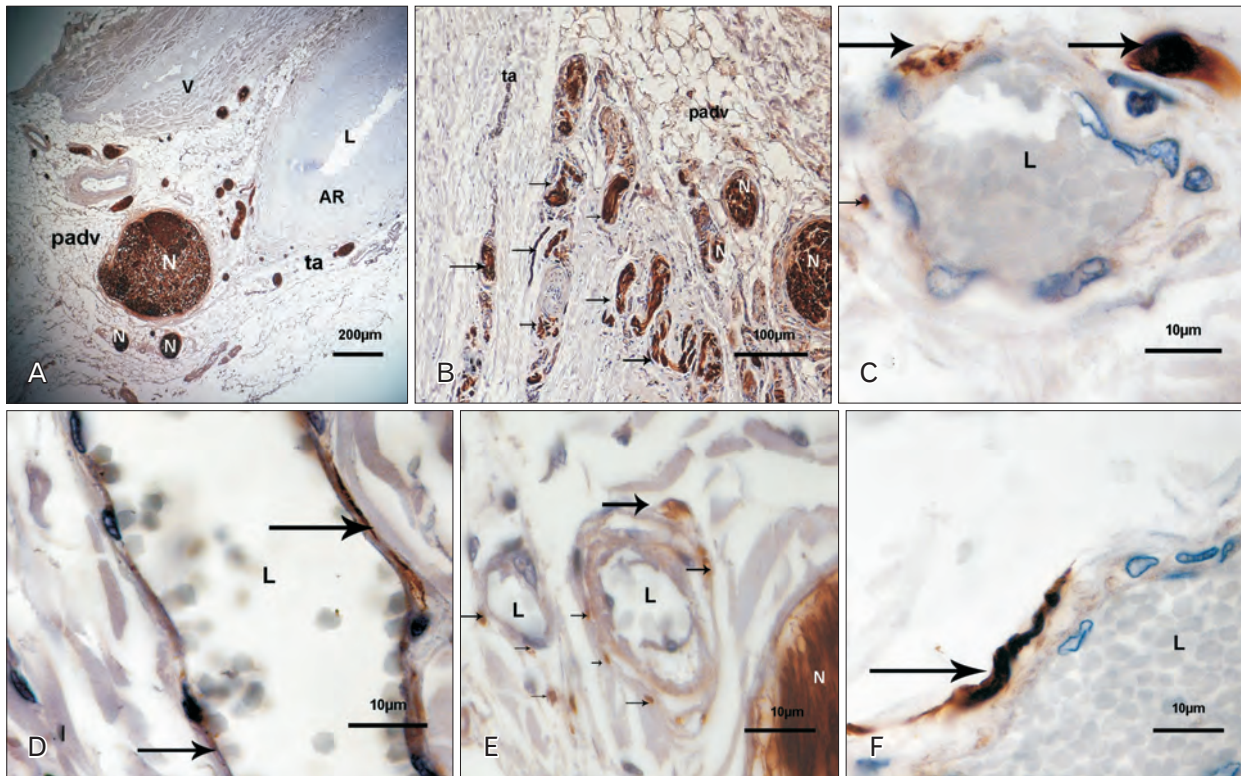The extracellular matrix constituted 73.4% (IR=14.2%) of

Fig. 2. Staining of nerve fibers with S100 in the adventitia and periadventitial tissue: (A) shows that most of the nerves are oriented transversely and run parallel to the vessels; (B) nerve fibers in the outer adventitia in relation to the vasa vasorum and transversely sectioned nerves are observed in the periadventitial tissue; (C) nerve fibers in relation to vasa vasorum transversely sectioned; (D) nerve fibers located in adventitial longitudinal vasa; (E) several nerve fibers are located in the vasa vasorum wall; (F) detail of a nerve fiber in the wall of a vasa vasorum longitudinally sectioned. Arrows indicate nerve fibers in the vasa vasorum wall. L, lumen; V, vein; AR, artery; ta, tunica adventitia; padv, periadventitial tissue; N, nerves. anti-S100 immunodetection. Bar in A: 200 µm, Bar in B: 100 µm, Bar in C–F: 10 µm.

the tunica media. This component was slightly higher in the left than in the right artery, without a significant difference. However, concerning the segments, the highest proportion of extracellular matrix appeared in the middle part of the artery, and this difference was nearly significant (Table 4).

The elastic fibers component of the extracellular matrix assessed between the inner and outer elastic membranes was 12.2% (IR=12.1%), with a slightly no significant higher percentage on the left than on the right side (Table 4).

However, the percentage of elastic fibers decreased significantly between the proximal and middle segments and between the proximal and distal segments, being the difference not significant between the middle and distal sectors (Table 4).

Tunica adventitia

The tunica adventitia was formed by connective tissue with elastic fibers located in several directions. Multiple vasa and nervi vasorum were present. The tunica adventitia ex-

tended toward fatty tissue in its outer part, putting it together with adjacent structures.

Outer elastic lamina

An outer elastic membrane sharing the adventitia from the tunica media was not well defined in the proximal segment of the renal artery (Fig. 1A, B). Therefore, the elastic layers in the media adventitia border changed along the artery to form a well-defined outer elastic membrane in the middle and distal segments of the artery (Fig. 1C–F).

Ganglia, nerves and nervous endings

In the surrounding arterial tissue beyond the outer part of the adventitia, small ganglia were observed and nerves profiles from the renal plexus were disposed parallel to the length of the artery (Fig. 2A, B). Smaller nerves and myelinated fibers went into the tunica adventitia. Myelinated fibers profiles were located in the walls of the vasa vasorum. S100-positive
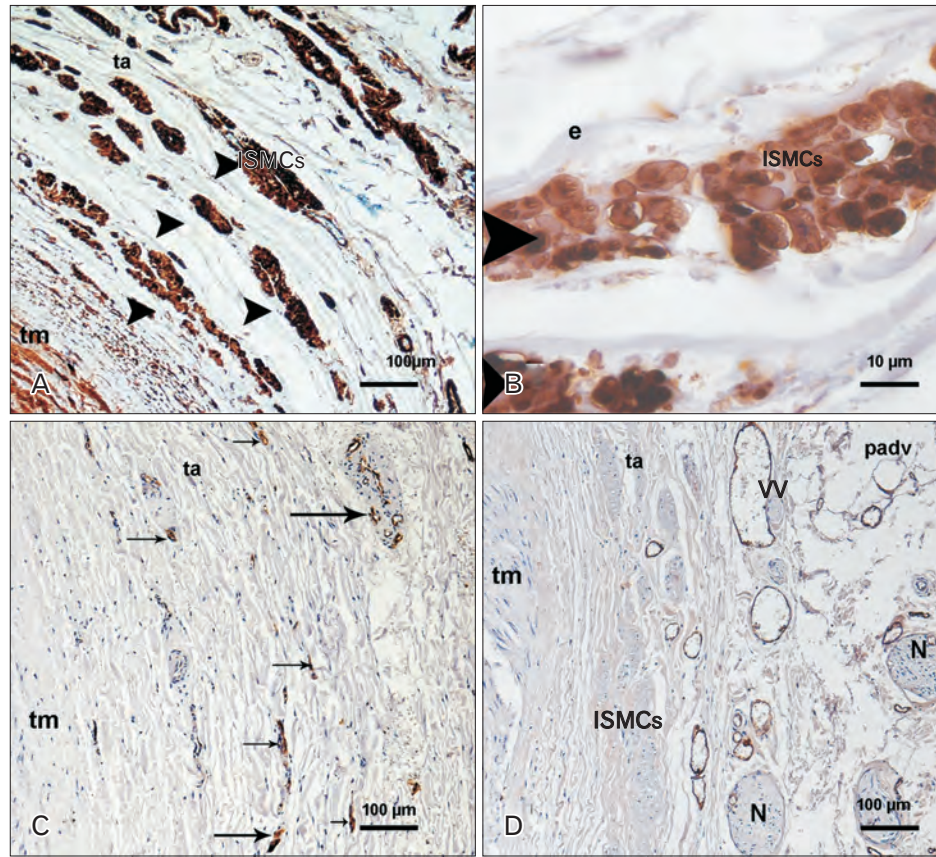
Fig. 3. Photomicrograph of the human renal artery wall. (A) and (B) show actin staining samples. (C) and (D) show von Willebrand factor staining (Bar in A, C, D: 100 μm, Bar in B: 10 μm). (A) Bunches of longitudinally oriented smooth muscle cells (SMCs) are surrounded by elastic fibers in the adventitia; the formations have a fusiform morphology; some of them have vasa vasorum (VV); (B) detail of one of the SMCs bunches; (C) endothelial cell of VV in the adventitia; most of the vasa have a disposition parallel to the lumen; (D) shows dilated VV in the adventitia. Arrows indicate VV. In addition, some nerves are observed in periadventitial tissue. tm, tunica media; ta, tunica adventitia; padv, periadventitial tissue; lSMCs, longitudinal SMCs formation; e, elastic layer; N, nerves.

fibers were not observed in other vascular tunica (Fig. 2C–F).

Smooth muscle cells

SMCs of longitudinal disposition were localized in the adventitia of the artery in 36 of 94 cases microscopically observed (38.3%). Bundles of SMCs were situated beyond the outer elastic membrane in the middle and distal segments of the arteries. Groups of SMCs formed fusiform structures located in a circular arrangement in the transverse section of the artery. They were surrounded by elastic fibers and other elements of the extracellular matrix. These cells were positive for actin immunolabeling (Fig. 3A, B).

Vasa vasorum

The vasa mostly had a circular disposition parallel to the vascular lumen in all segments of the artery (Fig. 3C, D).

Pathology in the arterial wall of the samples studied.

In our sampling, 37.9% (36) of the samples presented any grade of a pathologic irregular wall. Of these samples, 86.1% (31) presented an atheromatous plaque, and 13.9% (5) fibromuscular dysplasia. There was no difference between the right and left sides. Nevertheless, pathologic lesions depended on the segment, with an atheromatous plaque in proximal segments and fibromuscular dysplasia in more distal segments.

Discussion

The current study shows that the main renal artery originates in the aorta as an elastic artery and approaches the kidney as a muscular artery. A similar conclusion was drawn by Wright [9] and Osborne-Pellegrin [10] in renal arteries of

humans and rats. The findings of this study display for the first time that; the modification in the structure of the renal artery was accomplished by a significant decrease in the IM, tunica intima, and tunica media thickness from proximal to distal arterial segments, besides a modification in the proportion of the components of the extracellular matrix in the tunica media.

The samples showed a broader and more irregular tunica intima in the elastic part of the artery than in other more distal segments. The most expansive zones mainly corresponded to intimal cushions, which have been described as a consequence of vascular injury [27] and physiological intimal hyperplasia [28, 29].

Those intimal thicknesses are considered precursors for atherosclerotic plaque formation [30]. Therefore, our findings support that the atherosclerotic lesions would be more frequent in the proximal than in the middle and distal segments of the renal artery because of the tunica intima structure [31].

There was no difference in the tunica media between the right and the left renal arteries about the SMCs or extracellular matrix composition. Nor could we observe a significant difference in those components along the artery. The current study showed, however, an evident variation in the proportion of the ECM. The elastic tissue proportion of the extracellular matrix in the tunica media decreased from proximal to distal segments. A decrease in the elastic element along its length has also been described in the common carotid artery, and it has been considered a morphological adaptation of the tunica media to the stress in the artery [32].

The reduction in the elastic component along the artery entails an increase in the other components of the extracellular matrix as collagen and amorphous ground substance along the arterial length, and consequently a modification in the ratio between the elements of the extracellular matrix. This ratio is a valuable index of relative compliance for maintaining tension within the arterial wall. It seems crucial to the success of therapeutic procedures and predicts the response to some therapeutic techniques [33]. The results of this work support a possible different therapeutic arterial response attending to the sector of the artery used in the intervention.

Concerning the outer elastic membrane, Osborne-Pellegrin [10] described the persistence of an external elastic membrane in the renal artery only after the second arterial branching [10]. However, our results showed that the outer elastic lamina could already be seen in the middle third of the artery and that the elastic layers located between the SMCs in the proximal segment became less prominent toward the middle and distal arterial segments. The external elastic membrane showed differences depending on the disposition of the elastic lamina in the tunica media; the less elastic component the tunica media had the more elastic component the outer elastic membrane showed.

The renal artery wall receives its vascularization from; the external vascular supply of the aorta itself, the inferior suprarenal artery, or the diffuse vascular system of the retroperitoneal space, and from; the internal vascular supply of the renal artery itself [34]. In our samples, the vasa were abundant in the adventitia of normal renal arteries and were not observed in the tunica media except in pathologic samples.

We observed bunches of SMCs of longitudinal disposition in the loose part of the tunica adventitia. Those bunches appeared as fusiform and well-organized formations located in the transverse sections of the arteries. The first description of these formations was made by Osborne-Pellegrin [10] in the tunica adventitia of the renal artery of the rat, principally at branch points. More recently, longitudinally oriented cells were also described in the adventitia of the branching sites of coronary arteries of Sprague–Dawley rats, zebra finches, and lizards [35]. Those bunches have been considered the response to increased stress at the branch points and the considerable nervous control that the distal renal artery is under and whose activity regulates the blood supply to the kidney depending on the physiological conditions [10, 35]. However, our findings showed bunches of SMCs in the middle and distal segments of the renal arteries without relation to branching points; neither could we find myelinated axon profiles within those muscle strips except when they included vasa vasorum profiles.

Ábraham [36] suggested that the nerve supply of the renal arterial wall is richer than elsewhere in the organism, comparable only to the aortic arch in certain mammals. Our samples showed small S-100 positive nerve profiles in the loose part of the adventitia and more prominent nerves from the renal plexus running in the periadventitial tissue. Those nerves were mainly parallel to the artery, running toward the kidney or in an oblique disposition crossing the faces of the artery to join other nerves of the renal plexus [37]. In addition, S100-positive nerves profiles were observed in the wall of the vasa-vasorum with a likely function of regulation of blood flow [38]. The pathways that mediate vascular effects

on SNA on the vascular system have not been fully elucidated [39], and it is our consideration that the innervation of the vasa vasorum could have a role in that complex interrelation.

Limitations of the study

The analysis by sex and age was not possible because of the characteristics of the samples. Direct examination of collagen was not carried out, but it would be interesting to determine the exact ratio between the ECM in other studies. Although the data from our work about the pathologic lesions observed in our samples support the specific segmental distribution of vascular pathology in the renal artery, a large population should be studied to confirm this statement.

In conclusion, the main renal artery is a complex vessel that originates as an elastic artery and ends as a muscular blood vessel, changing the thickness of its wall and its extracellular matrix composition. Besides, numerous vessels and nerves are displayed in its tunica adventitia and periadventitial tissue. Those circumstances could be involved in a specific regional pathology setting and a different response to therapeutic procedures along the artery.

ORCID

Blanca Mompeó-Corredera:
https://orcid.org/0000-0003-4953-7653
Pablo Hernández-Morera:
https://orcid.org/0000-0002-0907-4765
Irene Castaño-González:
https://orcid.org/0000-0002-8188-7066
María del Pino Quintana-Montesdeoca:
https://orcid.org/0000-0003-1276-7594
Natalia Mederos-Real:
https://orcid.org/0000-0002-6549-5978

Author Contributions

Conceptualization: BMC. Data acquisition: BMC, NMR. Data analysis or interpretation: BMC, PHM, ICG, MdPQM. Drafting of the manuscript: BMC. Critical revision of the manuscript: BMC, PHM. Approval of the final version of the manuscript: all authors.

Conflicts of Interest

No potential conflict of interest relevant to this article was reported.

Acknowledgements

References

1. Dodd GD 3rd, Tublin ME, Shah A, Zajko AB. Imaging of vascular complications associated with renal transplants. AJR Am J Roentgenol 1991;157:449-59.
2. Hughes RJ, Scoble JE, Reidy JF. Renal angioplasty in non-atheromatous renal artery stenosis: technical results and clinical outcome in 43 patients. Cardiovasc Intervent Radiol 2004;27:435-40.
3. Kim HJ, Do YS, Shin SW, Park KB, Cho SK, Choe YH, Choo SW, Choo IW, Kim DK. Percutaneous transluminal angioplasty of renal artery fibromuscular dysplasia: mid-term results. Korean J Radiol 2008;9:38-44.
4. Liang P, Hurks R, Bensley RP, Hamdan A, Wyers M, Chaikof E, Schermerhorn ML. The rise and fall of renal artery angioplasty and stenting in the United States, 1988-2009. J Vasc Surg 2013;58:1331-8.e1.
5. Townsend RR, Mahfoud F, Kandzari DE, Kario K, Pocock S, Weber MA, Ewen S, Tsioufis K, Tousoulis D, Sharp ASP, Watkinson AF, Schmieder RE, Schmid A, Choi JW, East C, Walton A, Hopper I, Cohen DL, Wilensky R, Lee DP, Ma A, Devireddy CM, Lea JP, Lurz PC, Fengler K, Davies J, Chapman N, Cohen SA, DeBruin V, Fahy M, Jones DE, Rothman M, Böhm M. Catheter-based renal denervation in patients with uncontrolled hypertension in the absence of antihypertensive medications (SPYRAL HTN-OFF MED): a randomised, sham-controlled, proof-of-concept trial. Lancet 2017;390:2160-70.
6. Weber MA, Mahfoud F, Schmieder RE, Kandzari DE, Tsioufis KP, Townsend RR, Kario K, Böhm M, Sharp ASP, Davies JE, Osborn JW, Fink GD, Euler DE, Cohen DL, Schlaich MP, Esler MD. Renal denervation for treating hypertension: current scientific and clinical evidence. JACC Cardiovasc Interv 2019;12:1095-105.
7. Böhm M, Kario K, Kandzari DE, Mahfoud F, Weber MA, Schmieder RE, Tsioufis K, Pocock S, Konstantinidis D, Choi JW, East C, Lee DP, Ma A, Ewen S, Cohen DL, Wilensky R, Devireddy CM, Lea J, Schmid A, Weil J, Agdirlioglu T, Reedus D, Jefferson BK, Reyes D, D'Souza R, Sharp ASP, Sharif F, Fahy M, DeBruin V, Cohen SA, Brar S, Townsend RR. Efficacy of catheter-based renal denervation in the absence of antihypertensive medications (SPYRAL HTN-OFF MED Pivotal): a multicentre, randomised, sham-controlled trial. Lancet 2020;395:1444-51.
8. Okamura K, Satou S, Setojima K, Shono S, Miyajima S, Ishii T, Shirai K, Urata H. Reduction of blood pressure following after

renal artery adventitia stripping during total nephroureterectomy: potential effect of renal sympathetic denervation. Am J Case Rep 2018;19:567-72.

9. Wright I. The microscopical appearances of human peripheral arteries during growth and aging. J Clin Pathol 1963;16:499-522.

10. Osborne-Pellegrin MJ. Some ultrastructural characteristics of the renal artery and abdominal aorta in the rat. J Anat 1978;125(Pt 3):641-52.

11. Janzen J, Lanzer P, Rothenberger-Janzen K, Vuong PN. The transitional zone in the tunica media of renal arteries has a maximal length of 10 millimetres. Vasa 2000;29:168-72.

12. Janzen J. The microscopic transitional zone between elastic and muscular arteries. Arch Mal Coeur Vaiss 2004;97:909-14.

13. Hinata N, Suzuki R, Ishizawa A, Miyake H, Rodriguez-Vazquez JF, Murakami G, Fujisawa M. Fetal development of the mesonephric artery in humans with reference to replacement by the adrenal and renal arteries. Ann Anat 2015;202:8-17.

14. Mompeó B, Maranillo E, García-Touchard A, Sanudo JR. The morphogenesis of the renal plexus: renal artery and sympathetic fibers. Clin Anat 2019;32:272-6.

15. Abd Elrahim E. Computed tomography evaluation of renal artery morphometry in adults. The impact of age and gender. Saudi Med J 2020;41:34-7.

16. Singh G, Ng YK, Bay BH. Bilateral accessory renal arteries associated with some anomalies of the ovarian arteries: a case study. Clin Anat 1998;11:417-20.

17. Satyapal KS, Haffejee AA, Singh B, Ramsaroop L, Robbs JV, Kalideen JM. Additional renal arteries: incidence and morphometry. Surg Radiol Anat 2001;23:33-8.

18. Standring S. Gray's anatomy. The anatomical basis of clinical practice. 40th ed. Edinburgh: Churchill Livingstone; 2008.

19. Lee HB, Yang J, Maeng YH, Yoon SP. Bilateral multiple renal arteries with an extra-aortic origin and quadruple testicular veins. Anat Cell Biol 2019;52:518-21.

20. Leloup AJ, Van Hove CE, Heykers A, Schrijvers DM, De Meyer GR, Fransen P. Elastic and muscular arteries differ in structure, basal NO production and voltage-gated Ca(2+)-channels. Front Physiol 2015;6:375.

21. Borlotti A, Khir AW, Rietzschel ER, De Buyzere ML, Vermeersch S, Segers P. Noninvasive determination of local pulse wave velocity and wave intensity: changes with age and gender in the carotid and femoral arteries of healthy human. J Appl Physiol (1985) 2012;113:727-35.

22. Matz RL, Schott C, Stoclet JC, Andriantsitohaina R. Age-related endothelial dysfunction with respect to nitric oxide, endothelium-derived hyperpolarizing factor and cyclooxygenase products. Physiol Res 2000;49:11-8.

23. Dougherty G. Digital image processing for medical applications. Cambridge: Cambridge University Press; 2009.

24. Cordeiro de Amorim R, Mirkin B. Minkowski metric, feature weighting and anomalous cluster initializing in K-Means clustering. Pattern Recognit 2012;45:1061-75.

25. Shmmala FA, Ashour W. Color based image segmentation using different versions of K-Means in two spaces. Glob Adv Res J Eng Technol Innov 2013;1:30-41.

26. Witten IH, Frank E, Hall MA, Pal C. Algorithms: the basic methods. In: Witten IH, Frank E, Hall MA, Pal C, editors. Data Mining: Practical Machine Learning Tools and Techniques. 4th ed. Cambridge: Morgan Kaufmann Publishers; 2016. p.91-160.

27. Madri JA, Reidy MA, Kocher O, Bell L. Endothelial cell behavior after denudation injury is modulated by transforming growth factor-beta1 and fibronectin. Lab Invest 1989;60:755-65.

28. Stehbens WE. Focal intimal proliferation in the cerebral arteries. Am J Pathol 1960;36:289-301.

29. Yoro T, Burnstock G. Fine structure of "intimal cushions" at branching sites in coronary arteries of vertebrates. A scanning and transmission electron microscopic study. Z Anat Entwicklungsgesch 1973;140:187-202.

30. Stary HC, Blankenhorn DH, Chandler AB, Glagov S, Insull W Jr, Richardson M, Rosenfeld ME, Schaffer SA, Schwartz CJ, Wagner WD, Wissler RW. A definition of the intima of human arteries and of its atherosclerosis-prone regions. A report from the Committee on Vascular Lesions of the Council on Arteriosclerosis, American Heart Association. Arterioscler Thromb 1992;12:120-34.

31. Safian RD, Textor SC. Renal-artery stenosis. N Engl J Med 2001;344:431-42.

32. Kato Y, Mizutani T, Otsuka N, Ezure H, Inoue Y. Quantitative analysis of the elastic fiber in the tunica media at the carotid bifurcation. Okajimas Folia Anat Jpn 2018;95:23-7.

33. Sindram D, Martin K, Meadows JP, Prabhu AS, Heath JJ, McKillop IH, Iannitti DA. Collagen-elastin ratio predicts burst pressure of arterial seals created using a bipolar vessel sealing device in a porcine model. Surg Endosc 2011;25:2604-12.

34. Kurzidim MH, Oeschger M, Sasse D. Studies on the vasa vasorum of the human renal artery. Ann Anat 1999;181:223-7.

35. Kockx MM, Wuyts FL, Buyssens N, Van Den Bossche RM, De Meyer GR, Bult H, Herman AG. Longitudinally oriented smooth muscle cells in rabbit arteries. Virchows Arch A Pathol Anat Histopathol 1993;422:293-9.

36. Ábrahám A. Microscopic innervation of the heart and blood vessels in vertebrates including man. Oxford: Pergamon Press; 1969.

37. Mompeo B, Maranillo E, Garcia-Touchard A, Larkin T, Sanudo J. The gross anatomy of the renal sympathetic nerves revisited. Clin Anat 2016;29:660-4.

38. Williams JK, Heistad DD. Structure and function of vasa vasorum. Trends Cardiovasc Med 1996;6:53-7.

39. Chistiakov DA, Ashwell KW, Orekhov AN, Bobryshev YV. Innervation of the arterial wall and its modification in atherosclerosis. Auton Neurosci 2015;193:7-11.